Acoustic monitoring of thermo-mechanical tests

in a salt mine

Cyrille Balland and Anne Raingeard, Ineris, Nancy, France
Joël Billiotte and Bruno Tessier, School of Mines, Paris, France
Emmanuel Hertz, Salins du Midi, Varangéville, France
Grégoire Hévin, Storengy, Rueil-Malmaison, France

ACOUSTIC MONITORING OF THERMO-MECHANICAL TESTS IN A SALT MINE

Cyrille Balland and Anne Raingeard

National Institute for Industrial Environment and Risks, Nancy, France

Joël Billiotte and Bruno Tessier,

School of Mines, Paris, France

Emmanuel Hertz,

Salins du Midi, Varangéville, France

Grégoire Hévin,

Storengy, Rueil-Malmaison, France

Abstract

The natural gas storage in salt caverns requires faster injection cycles / racking due to the increasing dynamics of the energy market. These cycles induce rapid changes in the internal pressure of the stored gas causing important temperature changes that can damage the rock salt mass. Several theoretical studies have been conducted to estimate this type of damage (Brouard et al, 2011; Sicsic and Berest, 2014). To experimentally observe this damage, the Solution Mining Research Institute (SMRI) has cofounded the Starfish project between 2013 to 2016 and led by Storengy in partnership with the Ecole des Mines de Paris, the Salins du Midi and INERIS. The main objective of this project was to initiate and characterize the damage by purely thermal stresses at the surface of a large bloc of salt partially slotted in a rock mass of the salt Mine of Varangéville (France). This was to determine the type of failure mechanism involved, the nature and extent of the cracks induced, as well as amplification of the damage of the solid mass with repeated cooling cycles.

The salt being favorable to the generation of Acoustic Emissions (AE) and the propagation of the stress waves, the acoustic monitoring method has been chosen to follow the impact of the salt cooling. In addition to thermal and mechanical sensors, an acoustic monitoring device consisting of 16 ultrasonic sensors has been installed on the free surface and in boreholes. It enabled to record and locate a large number of AE (58426) with good accuracy (2.5 cm). Those AE can be correlated to the evolution of salt fracturing. Acoustic monitoring provided a very good insight in the physics of the damaging process.

Key words: Instrumentation and Monitoring, Seismic, Underground mine, Gas Storage, Rock Mechanics, France

Introduction

Natural gas storage in salt caverns requires increasingly rapid injection/draw-off cycles due to the increasingly dynamic energy market. These cycles are accompanied by rapid fluctuations in the internal pressure of the stored gas, but also by major temperature variations that may damage the salt deposit. This type of thermal damage due to gas expansion has been observed in the case of a granite formation

(Lee et al, 1982). Several theoretical studies have been carried out to estimate this type of damage in the salt (Brouard et al, 2011; Sicsic et Berest, 2014). In order to observe this damage experimentally, the SMRI (Solution Mining Research Institute) selected the Starfish project run by Storengy in partnership with the Paris School of Mines, Salins du Midi and INERIS. The purpose of this project is to cool down a salt deposit to reproduce the forces applied by the facing of a gas store. The main purpose was to initiate and describe the damage caused to the surface of the deposit by forces of a purely thermal origin. It involved finding out the type of fracture mechanism that occurred and the nature and extent of the fractures. It also involved highlighting or not highlighting possible regression or amplification phenomena damaging the deposit with repeated cooling cycles.

Most of the study was carried out in partnership between the parties involved in the project. However, several tasks were performed specially, in particular excavation and development of the mine gallery by CSME, designing and setting up the cooling system, visual monitoring, part of the geotechnical monitoring by the Paris School of Mines and finally a second part of the geotechnical and acoustic monitoring by INERIS. This second part is presented in this study report. However, a brief presentation of the site and the cooling system has been added in advance to make it easier to understand the rest of the study. This presentation and the mechanical aspect of the physical phenomena will be developed in the reports from the partners. A summary including the different approaches will be set out in the final overall project report.

Acoustic monitoring of the damage to rock deposits has been used several times in the course of compression tests. King et al. (1997) highlighted a correlation in the laboratory between acoustic emissions (AE) and fracture density during triaxial tests on the sandstone. Dahm (2001) and Moriya et al (2005) studied acoustic activity in the salt. They demonstrated that this material shows a high degree of acoustic activity under mechanical forces with shear mechanisms and minor attenuation of the mechanical waves due to its crystalline structure. Acoustic emissions of thermal origin were studied essentially during warming phases that exceeded the thermal amplitude expected in gas storage: 550°C in salt for Dahm (1998), 200°C Vasin et al (2006) in marble and sandstone or 800°C in concrete for Tang (2015). Dahm and Vasin indirectly studied acoustic emissions during cooling phases after preliminary warming. They demonstrated that acoustic activity reached a peak when cooling began, i.e. when the heat source was cut off. However, this comparison is limited, as the damage mainly took place during the warming phase. The Starfish experiments could have followed a similar, and hence better known protocol, but it was more important to control the cooling phase than the warming phase.

As salt is a favourable medium for the generation of acoustic emissions and propagation of their signals, the acoustic monitoring method was chosen for monitoring the cooling of the salt. It is expected that this method will make it possible to quantify and locate the damage in the stressed deposit. Several special methods were used in this study for locating acoustic emissions and estimating their magnitude and mechanisms. The implementation of the study and the results obtained are set out in this report.

Experimental array

The experimental site is located in a blind gallery in the Varangéville salt mine excavated for this purpose by the operator, Salins du Midi (Figure 1). The experiment covers a 10 m² area of the salt deposit at the most homogeneous location in the gallery. In particular, the experiment had to take place at a distance from the walls and avoid the drying cracks that formed at the time when the salt was deposited to avoid introducing any mechanical discontinuities. The area was subdivided using a cutter, then smoothed by the operator CSME for easier observation and for fitting various sensors.

This salt is mineralised on a macroscopic level with centimetre-sized crystals. Its mean density is 2.2. The Young's and Poisson's moduli of the salt are 25 GPa and 0.25 respectively, with a uniaxial compressive strength of 30 MPa and a tensile strength of 1 to 3 MPa. Its expansion coefficient is 38 µdef/°C. The cooling chamber was installed by Armines on this prepared area. The cooling chamber comprises five insulated walls with two access doors; the cooling unit in the corner is on the ceiling and the ventilator unit is in the west corner on the ground.
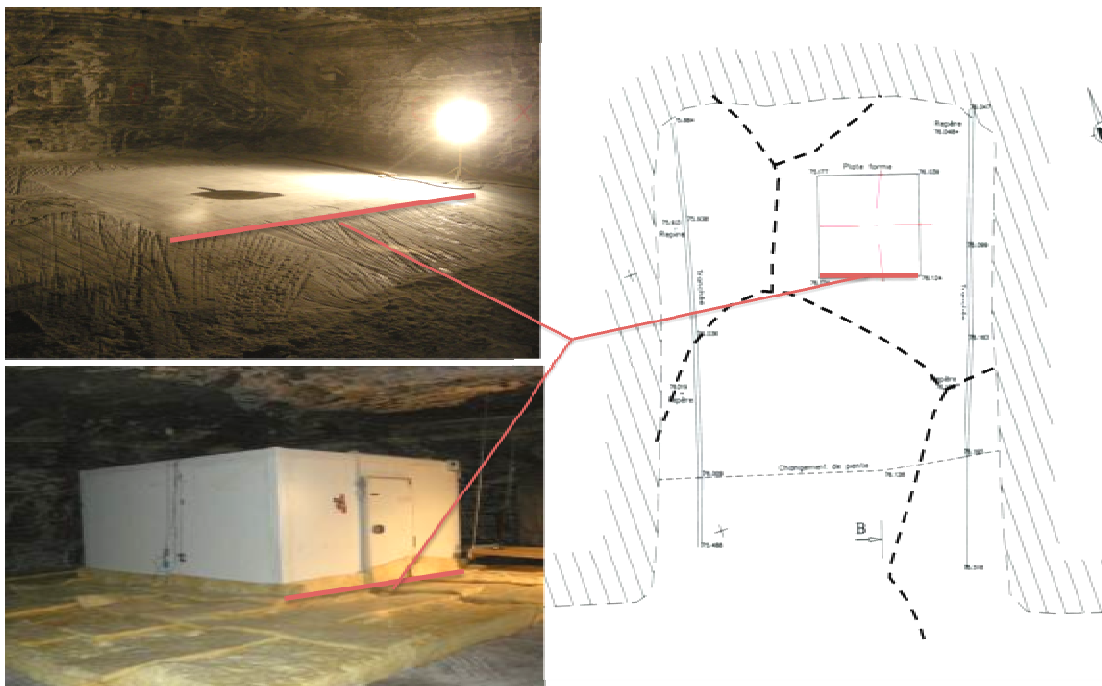
Figure 1. Location of the deposit and position of the cooling chamber (ARMINES) in a Varangéville mine gallery (Salins du Midi) with decompressive trenchs on the sides (parallel lines) and shrinkage slot (dotted line).

The ultrasonic array comprises 16 piezoelectric sensors arranged either on the surface, adhering to the salt deposit or embedded in the walls of 5 boreholes. Eleven sensors work as receivers and 5 others work as transmitters. The transmitters are connected to a special box that can emit 500 volt pulses, while the receivers are connected to the Hyperion acquisition centre with a maximum sampling frequency of 5 MHz. The ultrasonic sensors are R6α type resonant sensors. They all have an equivalent instrument response with a peak frequency centered on the 60 kHz frequency band.

The ultrasonic array is centered in the cooling chamber in order to monitor the most homogeneous section. The purpose was to avoid potential edge effects due to the ventilators, walls and doors. Receivers R1, R2, R3 and R4 are located at a depth of about 60 cm at the bottom of the four inclined boreholes and at about 70 cm from the centre of the array. Receivers R5, R6, R7 and R8 are laid out on the surface at the four corners of a 2 m x 2 m square (Figure 2). The four transmitters E1, E2, E3 and E4 are inserted at the center of the sides of this square. Transmitter E5 and receiver R9 are placed on the surface at the centre of the array. Receivers R10 and R11 are located at 20 and 40 cm respectively in the central borehole.

The surface sensors are glued and face downwards. The two sensors in the borehole are sealed and face horizontally towards sensor E2, while each of the oblique borehole sensors face the top of the borehole perpendicular to the boreholes (25°), i.e. inclined at about 65° on the axis of each borehole.
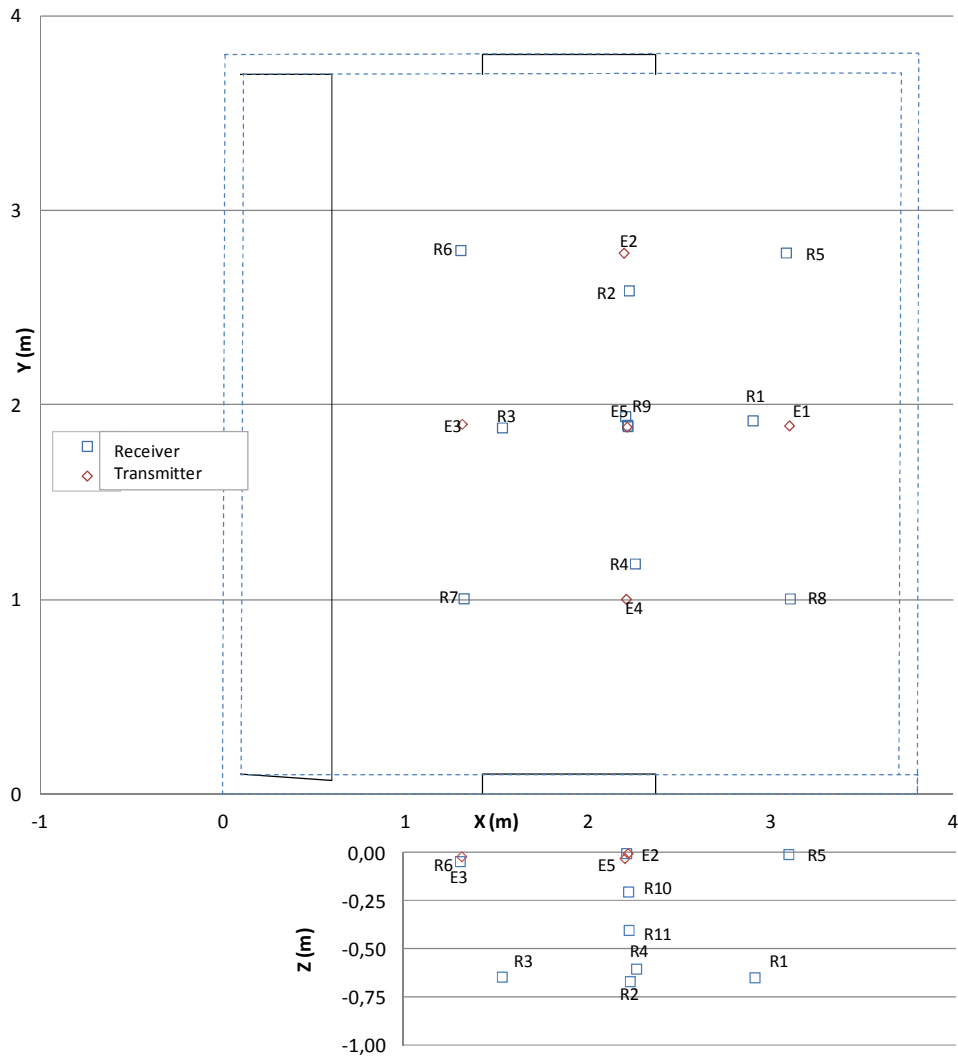
Figure 2. Location of the ultrasonic sensors

Acoustic emissions were located by analysing the time taken for the acoustic emission to reach the 11 sensors. Taking account of the number of registered acoustic emissions (several tens of thousands), it is impossible to tally these wave arrivals manually. They are therefore tallied automatically by means of an a specific algorithm.

Localisation was optimised with emissions from the 5 piezoelectric transmitters in the monitoring array with an average wave velocity P calculated at 4457 m/s. As the positions of the events were precisely known, the location parameters could be adjusted. In order to compare the different localisation methods, the X, Y and Z differences between the measured location and the known location of the transmitters was calculated for each location. The localisation method gives an error around 2.5 cm.

Acoustic activity

The salt deposit was subjected to 4 cooling cycles with a set point temperature in the cooling chamber of -9°C over a minimum period of 28 days for the first 3 cycles. The main purpose was to compare how the damage develops as the cooling cycles progress. The warming phase between cooling cycles varies (from 1 month for the 1st to 3 months for the 2nd and 3rd cycle) (Figure 3) as it is not controlled and is

accompanied by substantial condensation which required the surface and the sensors to be systematically reconditioned. The last cooling phase not planned in the experiments took place in two stages, one of them still lasting 14 days at -9°C and the other during 22 days at -27°C. The main purpose of this last cycle was to monitor the damage under increased stress.
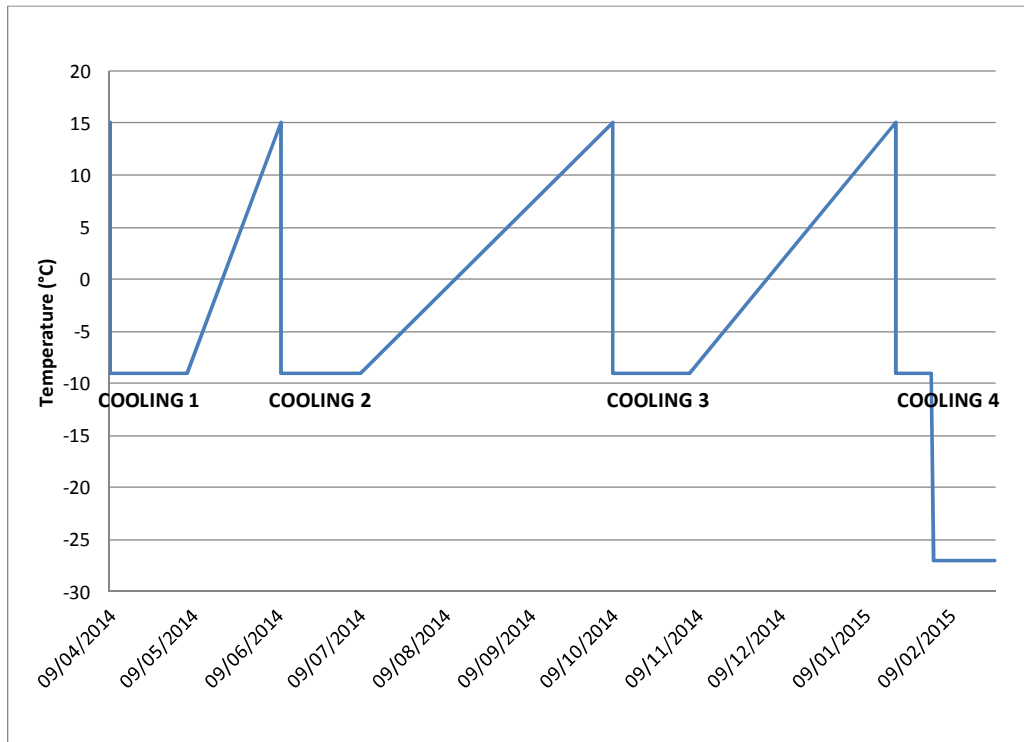

Figure 3. Distribution of cooling cycles with time

During the four cooling cycles, 58,426 acoustic emissions were registered. The number of acoustic emissions recorded was greatest for the first cooling cycle, with 21,614 emissions, and least for the third cooling cycle, with 8124 emissions. The number of acoustic emissions would probably have been considerably greater in the first cooling cycle if the acquisition system had not reached its saturation level. By extrapolating the first 143 minutes, the total number of acoustic emissions in the first cooling cycle would approach 47,000 to 60,000, depending on whether the second or the third cooling cycle is used for extrapolation.

In Figure 4, the 4th cooling cycle has been split into two cooling cycles, 4' and 4", so as to be able to extract the first stage at -9°C identical to the first 3 cooling cycles. The total number of acoustic emissions is nevertheless not comparable over the entire period, as the cooling cycle only lasted half as long as the 3 others, i.e. 14 days. Cooling cycle 4' can nevertheless be compared to the other cooling cycles over the first twelve hours (cycle 2 and 3) and over the first 143 minutes (cycles 1, 2 and 3). These two periods show that the activity increased in the 4th cooling cycle at an intermediate level between cooling cycles 2 and 3. Finally, the general trend of the activity is towards reduction according to a power law.
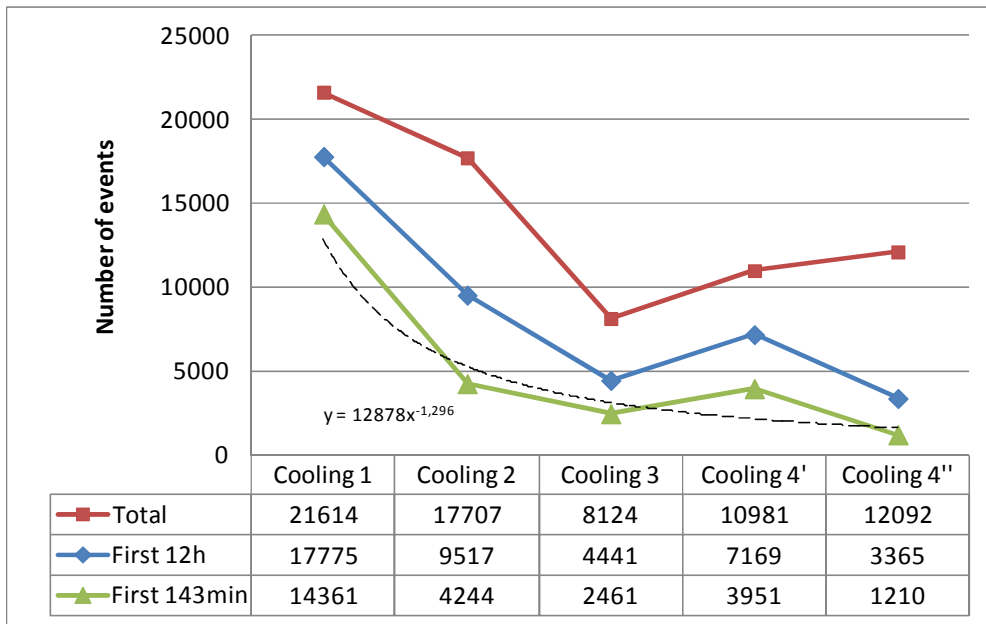
Figure 4. Changes in the number of events at the end of each cooling period.

During the cooling period of all cycles, the activity was strongest initially (Figure 5); more than 54% of the acoustic emissions had already taken place during the first 12 hours of cycles 2 and 3. After 3 days, this accounted for almost 80% of the acoustic emissions. The trend is the same for cooling cycle 4', although the overall duration is shorter.

The shape of the curve for cooling cycle 4" at -27°C is different: there are less acoustic emissions at the start; after 12 hours, only 27% of the acoustic emissions have been produced despite the fact that the total duration of the cycle is shorter. This difference should be viewed in parallel with a slower temperature reduction for the -27°C set point than for the -9°C one in the previous cycles.
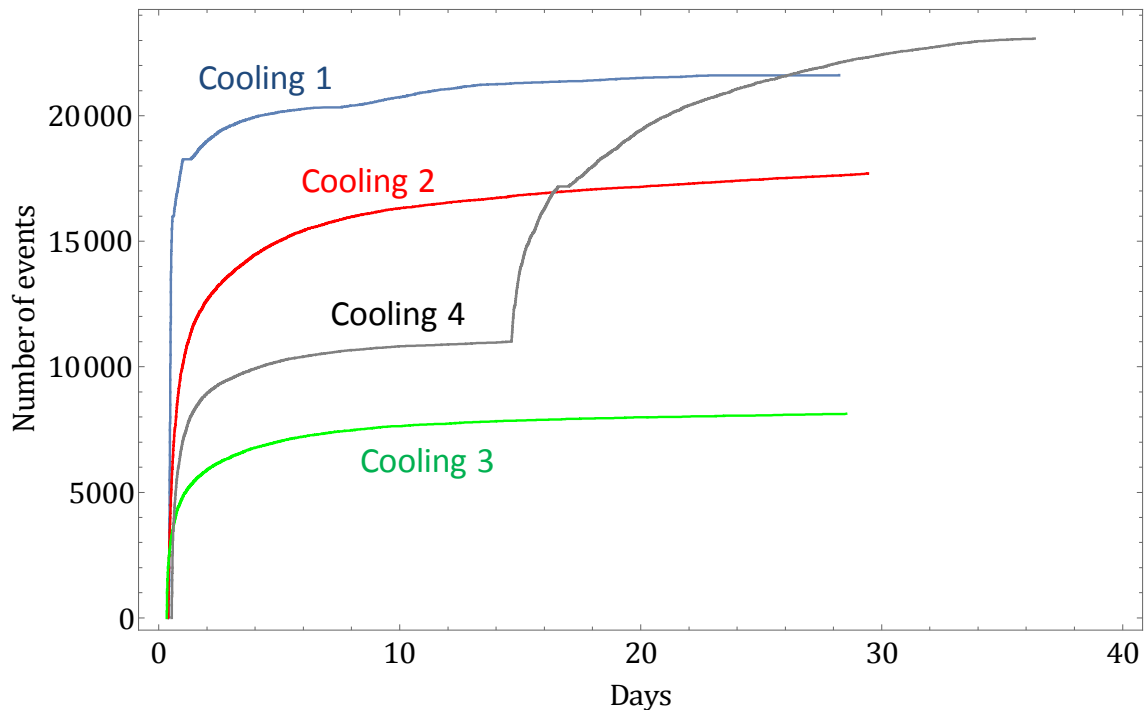
Figure 5. Number of acoustic emissions during the 4 cooling cycles (cooling cycle No 1: blue; cooling cycle No 2: red; cooling cycle No 3: Green; cooling cycle No 4 (4' and 4"): grey).

The distribution of this activity was analysed after the level of acoustic activity. For this purpose, all acoustic emissions with at least 10 tallied signals were located. This corresponds to 40,490 acoustic emissions out of a total of 58,426, i.e. 69%. The mean uncertainty in the pulse localisation is 2.5 cm. This is probably of the same order for the acoustic emissions or even better, as the signals are stronger than the pulses summed up 100 times. The first arrival of the acoustic emissions is therefore better defined than that of the pulses with efficient automatic tallying. Checks on a sample of signals showed that automatic tallying was occasionally poor on one or two signals when the acoustic emissions had a low amplitude. This rate is estimated at 5%. Localisation is therefore more precise for stronger acoustic emissions.

The results of these localisations for the 4 cycles are shown for during the 1st hour (Figure 6) and. During the 1st hour most of the acoustic emissions were located in a 20 cm thick surface strip. During the 2nd hour most of the acoustic emissions appear to increase in depth, with a more pronounced effect in the left half of the array nearer the ventilators, producing a spread, slightly inclined at an estimated 2° for cycle 1 towards the ventilators (towards the West). There is also a displacement to the East from the most dense centre of the spread as the cycles progress.

Taking the depth of the acoustic emissions more accurately in relation to time for each of the cycles (Figure 7), the increase in depth shows up more clearly. With time, the acoustic emissions follow each other in time at widely scattered depths. However, with a moving average of 10 acoustic emissions, then of 100 acoustic emissions, the average depth of each cycle follows a relatively uniform curve towards the stages at -0.90 m, -0.74 m, -0.71 m and -0.72 m respectively for cycles 1, 2, 3 and 4. Cycle 1 acoustic emissions thus propagate at a greater depth than those from the other cycles. They are concentrated in the first 143 minutes. It is possible to estimate the vertical migration velocity of the spread of acoustic emissions at the beginning of the cooling cycle, from 8 to 10 cm/hour depending on the cycle.
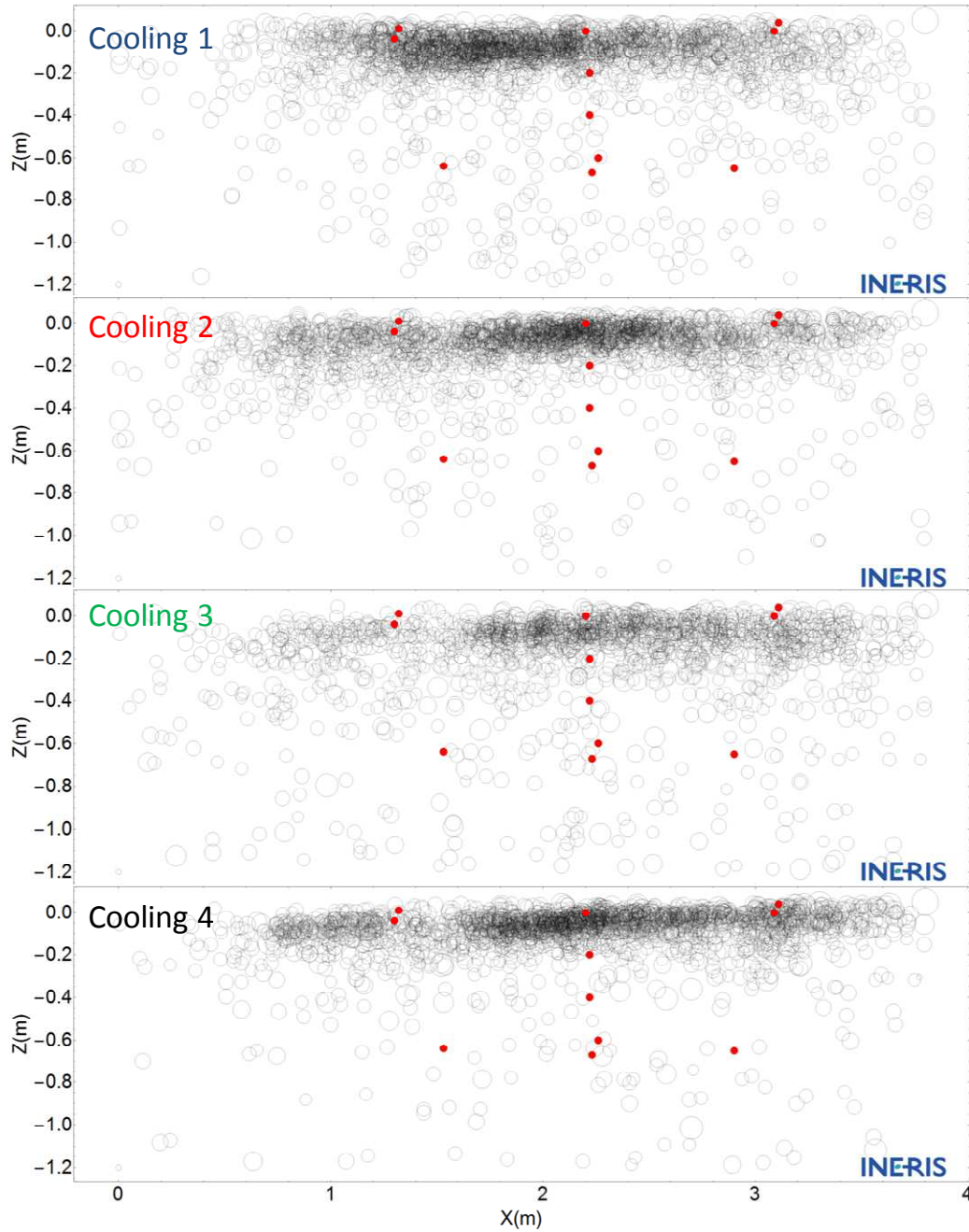
7

Figure 6. Location of acoustic emissions during the first hour on the 0XZ plane (the vertical plane perpendicular to the axis of the ventilators) in the 4 cooling cycles (from the top downwards). The magnitude is proportional to the diameter of the circles and two scales are placed on each graph: Magnitude -8 at the bottom left and Magnitude -3 at the top right.
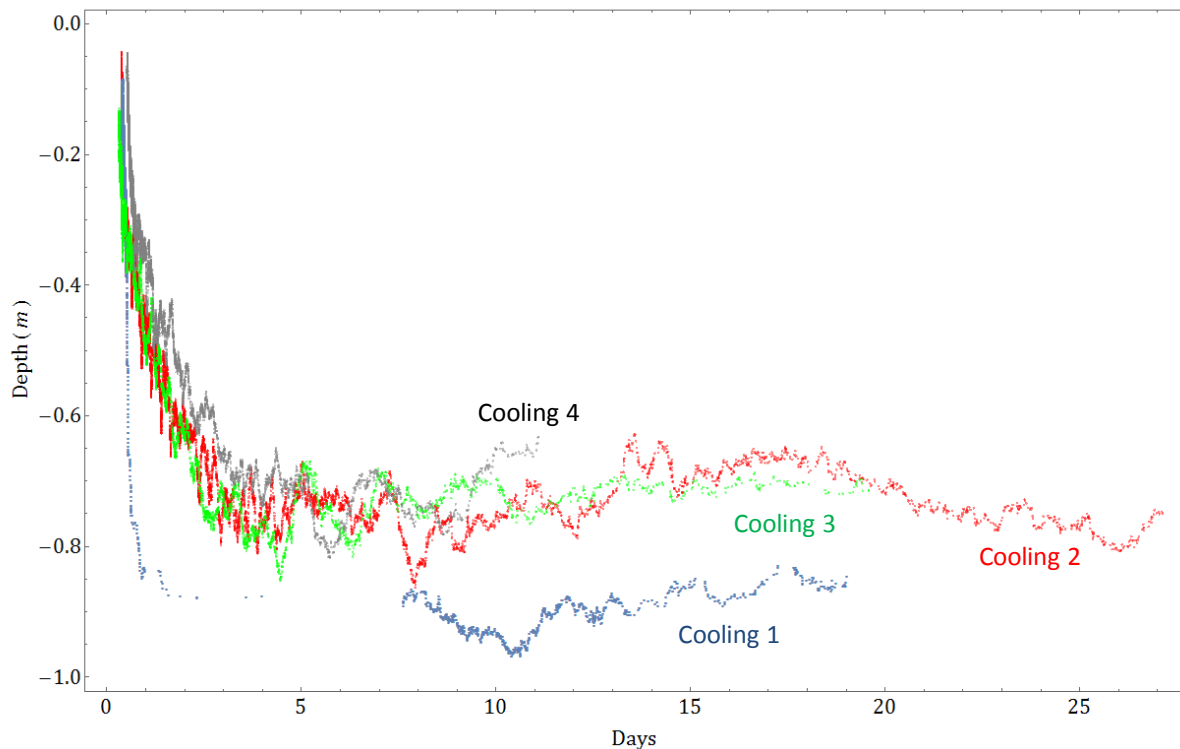
Figure 7. Variation in the depth of acoustic emissions during the 4 cooling cycles, moving average values of 100 acoustic emissions.

Conclusion

The acoustic monitoring array recorded and located a large number of acoustic emissions (58,426) with a relatively low level of uncertainty (2.5 cm). This provides a good representation of how fracturing develops in the salt. This acoustic monitoring provides several important results in response to the main questions raised about the nature of the rock salt and the extent of the damage.

Acoustic activity is greatest at the start of each cooling cycle, then diminishes with time to reach a very low level (background) after about 15 days. This activity diminishes asymptotically from one cycle to another in terms of the number of acoustic emissions and magnitude. With the surface temperature imposed at -9°C considering that the natural temperature in the mine is 15°C, the average depth attained by the acoustic emissions is about 90 cm during 1st the cooling period. For subsequent cycles, this depth is limited between 71 to 74 cm.

Most AE have a magnitude of around -5, which corresponds to radius of the fracture from 2 to 3 cm equivalent to the average size of the solid salt crystals. The results also shows that salt fracturing is mainly diffuse along the cold front spreading in agreement with the crazing observed on surface around the salt crystals with camera and other visual methods. All these results show that the first cooling strategy is critical since it generates the strongest and deepest AE. It will be interesting in the future to compare different salt cooling velocities and the impact on the maximum amplitude and the maximum depth of the EA. Such a crescendo could be an interesting operating mode for an operator to minimize the damage of his storage.

9

References

Aki and Richards, (1980), Quantitative Seismology: Theory and Methods W.J. Freeman & Co, San Francisco (1980)

Brouard B., Frangi A., Bérest P. (2011) – Mechanical stability of a cavern submitted to high-frequency cycles. SMRI Spring Meeting, Galveston, Texas, 99-116.

Dahm, T., Manthei, G,. Eisenblätter J., 1998, Relative moment tensors of thermally induced micro-cracks in salt rock, Tectonophysics, 289, pp. 61–74

Dahm T., (2001), Rupture dimensions and rupture processes of fluid-induced micro-cracks in salt rock, Journal of Volcanology and Geothermal Research, Volume 109, Issues 1–3, Pages 149-162

Gutenberg et C. F. Richter (1949). Seismicity of the earth and associated phenomena. Princeton University Press, Princeton, New Jersey

King MS, Shakeel A, Chaudhry NA. , 1997, Acoustic wave propagation and permeability in sandstones with systems of aligned cracks. Development in Petrophysics, No. 122

Lee C.,Tsui K, Tsa A., (1982) Thermomechanical response of a disposal vault in a high horizontal stress field. In: Witke W, editor .Proceedings of ISRM Aachen, Balkema;.p.961–9.

Moriya H., Fujita T., Niitsuma H., Eisenblatter J., Mantheib G., (2006), Analysis of fracture propagation behavior using hydraulically induced acoustic emissions in the Bernburg salt mine, Germany, International Journal of Rock Mechanics & Mining Sciences 43 49–57

Sicsic P., Bérest P., (2014), Thermal cracking following a blowout in a gas storage cavern, International Journal of Rock Mechanics & Mining Sciences 71 320–329

Tang, S.B., Tang, C.A., 2015, Crack propagation and coalescence in quasi-brittle materials at high temperatures, Engineering Fracture Mechanics, Volume 134, January Pages 404-432

Vasin R.N., Nikitin A.N., Lokajicek T., Rudaev V., 2006, Acoustic Emission of Quasi-Isotropic Rock Samples Initiated by Temperature Gradients, Physics of the Solid Earth, Vol. 42, No. 10, pp. 815–823